EXPERIMENTAL STUDY OF TURBULENT FLOW IN A VERTICAL DOUBLE SLOT FISHWAY: INFLUENCE OF FLOW DISCHARGE AND SLOPE

Anne Fleur Lejeune, Damien Calluaud, Gérard Pineau, Laurent David, Pierre Sagnes, Sylvain Richard

EXPERIMENTAL STUDY OF TURBULENT FLOW IN A VERTICAL DOUBLE SLOT FISHWAY: INFLUENCE OF FLOW DISCHARGE AND SLOPE

ANNE-FLEUR LEJEUNE
Institut Pprime, CNRS - Université de Poitiers, Isae-Ensma, Ecohydraulics Team, OFB-IMFT-PPRIME
11 boulevard Marie et Pierre Curie, BP 30179, Futuroscope Chasseneuil, FR86962, France

DAMIEN CALLUAUD
Institut Pprime, CNRS - Université de Poitiers, Isae-Ensma, Ecohydraulics Team, OFB-IMFT-PPRIME
11 boulevard Marie et Pierre Curie, BP 30179, Futuroscope Chasseneuil, FR86962, France

GÉRARD PINEAU
Institut Pprime, CNRS - Université de Poitiers, Isae-Ensma, Ecohydraulics Team, OFB-IMFT-PPRIME
11 boulevard Marie et Pierre Curie, BP 30179, Futuroscope Chasseneuil, FR86962, France

LAURENT DAVID
Institut Pprime, CNRS - Université de Poitiers, Isae-Ensma, Ecohydraulics Team, OFB-IMFT-PPRIME
11 boulevard Marie et Pierre Curie, BP 30179, Futuroscope Chasseneuil, FR86962, France

PIERRE SAGNES
Office Français de la Biodiversité (OFB), Direction de la recherche et de l'appui scientifique, Ecohydraulics Team, OFB-IMFT-PPRIME
Institut de Mécanique des Fluides, Allée du Professeur Camille Soula, 31400 Toulouse, France

SYLVAIN RICHARD
Office Français de la Biodiversité (OFB), Direction de la police et du permis de chasser, Ecohydraulics Team, OFB-IMFT-PPRIME
Institut de Mécanique des Fluides, Allée du Professeur Camille Soula, 31400 Toulouse, France

The Vertical Double Slot Fishway (VDSF), has not been the subject of many studies and is looked into here. This paper presents an experimental study of the influence of slope and flow discharge on the turbulent flow occurring inside the pools of a VDSF. The rise of the flowrate and the decrease of the slope both involve an increase in water depth inside the pool. As for the velocity magnitude and the turbulent kinetic energy, while the variation of the flowrate does not seem to impact significatively the values at mid-water depth, it is not the case with change of slope. As the slope gets steeper, so does the velocity and the turbulent kinetic energy throughout the pool.

1 INTRODUCTION

In October 2000, the Water Framework Directive was adopted by the European Union, and dictates that, among other things, all member states must restore the ecological continuity in rivers. It transpires with obstacles removal, their height reduction, facilities management or the creation of bypass structures, such as fishways. Numerous sorts of fishways have been implemented throughout the world, such as artificial rivers or pool fishways. The principle of the latter is based on dividing a fall to several successive smaller and more fish-accessible falls.

Among pool type fishways, one of the most employed is the vertical slot fishway (VSF), which has been the subject of many studies, both experimental (Ballu et al., 2019; Bombač et al., 2015; Calluaud et al., 2014) and numerical (Ballu, 2017; Bombač et al., 2014; Klein & Oertel, 2016; Stamou et al., 2018; Zhao et al., 2022). However, this kind of fishway, with a single slot, is derived from the vertical double slot kind, developed for the Hell's Gate canyon, on the Fraser river in Canada in 1943 (Clay, 1995). Although this kind was implemented first, few studies have been conducted specifically on vertical double slot fishways (VDSFs). Fujihara et al. (2003) compared the flow occurring inside three different types of VSF and one type of VDSF. In 2020, a

preliminary study was published comparing three fishways: a one-side VSF, an alternating side VSF and a VDSF (Huang, 2020).

The present study focuses solely on a vertical double slot fishway and the influence of flow discharge and slope on the turbulent flow occurring inside its pools. The results and conclusions were drawn from experiments carried out in a laboratory fishway.

2 MATERIALS AND METHODS

2.1 Experimental setup

The experiments were carried out in a laboratory prototype in the Pprime Institute Laboratory of the University of Poitiers (CNRS), France (Figure 1). This scale prototype is a 1:6 scale model, using the Froude similarity, of an existing VDSF, located at the Malause dam, on the Garonne River (France). The prototype is composed of 5 pools. The water is pumped from the downstream tanks (a) to the upstream one (b). The water then moves through the pools of the fishway (c) by gravity and finally discharges back into the downstream tanks (a), over a sash window (d) designed to even out the depth of water in each pool.

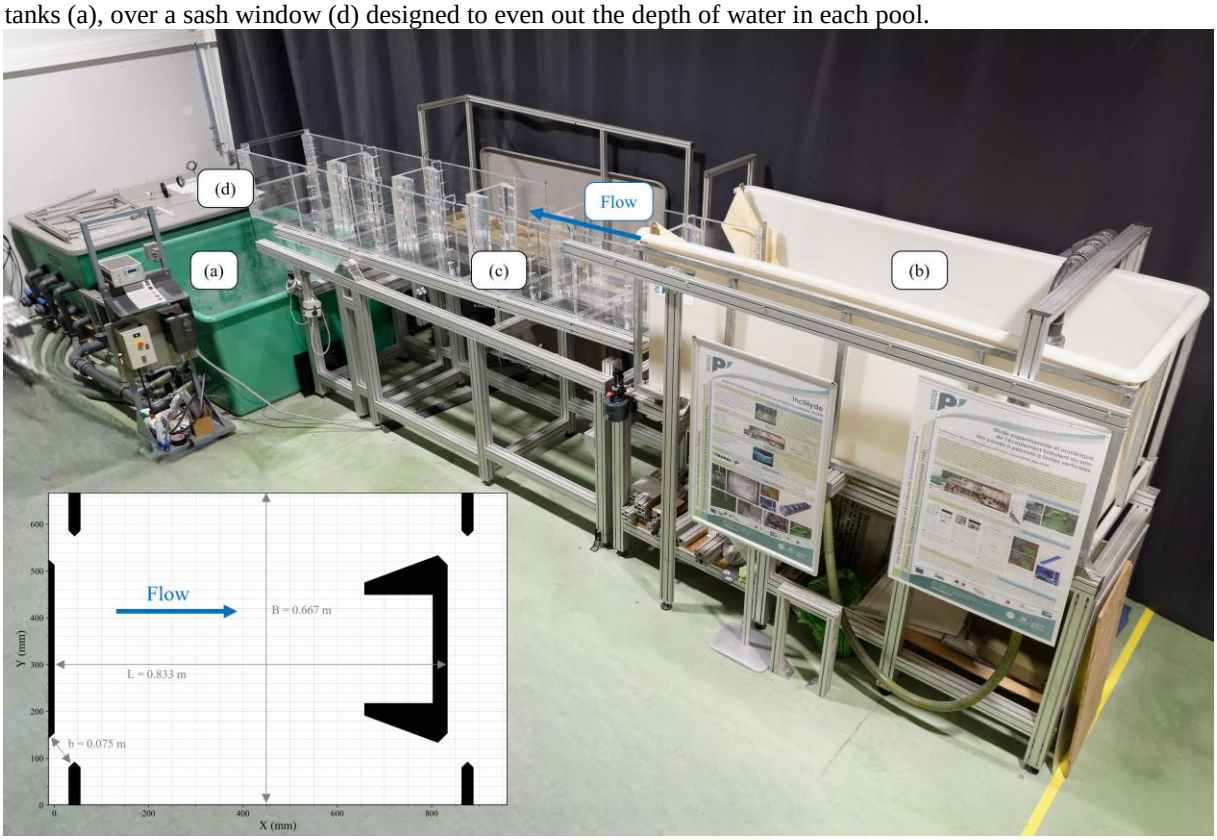

Figure 1. Experimental 1:6 scale vertical double slot fishway. The inset (bottom left-hand side corner) shows the geometry of a pool, seen from above

The X-axis is in the streamwise direction (see graph in the bottom left-hand corner of Figure 1). The origin of the pool is located behind the central baffle of the previous pool and the length of the pool is L = 0.833 m. The width of the pool is B = 0.667 m (in the Y direction). The unit width of the slots is b = 0.075 m. The studied slopes are s = 4%, 5% and 7.5% and the studied flow discharges Q = 0.023 $m^3 \cdot s^{-1}$, 0.027 $m^3 \cdot s^{-1}$ and 0.034 $m^3 \cdot s^{-1}$. The reference configuration (set from the observations of the in-situ VDSF of Malause) is defined by a slope of s = 4% and a flow discharge of Q = 0.034 $m^3 \cdot s^{-1}$. The experiments are undertaken in the middle pool, in order to insure the full development of the flow.

2.2 Experiments description

Three different kinds of experiments were implemented. The water depth in the pools for every configuration was measured, as well as the velocity with two approaches: 2D-velocity was recorded on whole planes using

Particle Image Velocimetry (PIV) and 3D-velocity was recorded on specific profiles throughout the pool with an Acoustic Doppler Velocimeter (ADV).

The water depth was recorded in the middle of the pool (X = L/2, Y = B/2) using acoustic probes. The sampling rate was of 200 Hz over a time period of 420 s. The distortion of the free surface and the droplets caused several losses of the signal during the acquisition, resulting in aberrant data. A velocity filter was thus applied to the signal in order to set aside erroneous values, like in previous fishway studies (Ballu, 2017).

The three components of the velocity were recorded on specific profiles using an Acoustic Doppler Velocimeter (ADV), in order to obtain the average velocity and the turbulent kinetic energy. The sampling rate of the ADV was 50 Hz over a 300 s acquisition time, which is sufficient for statistics data. A phase-space filter was used to remove aberrant values since it is the most suitable filter for these type of data (Goring & Nikora, 2002). The data were recorded on a transversal profile (C) located after the two slots, at X/b = 2.36 and Z/b = 2. The 3D time-average velocity magnitude (1) and 3D turbulent kinetic energy (2) were calculated as given below:

$$\overline{||V||_{3D}} = \sqrt{\overline{V_x(x,y,z)} + \overline{V_y(x,y,z)} + \overline{V_z(x,y,z)}} \quad (1)$$

$$k_{3D} = \frac{1}{2}\left(\sigma_x{}^2(x,y,z) + \sigma_y{}^2(x,y,z) + \sigma_z{}^2(x,y,z)\right) \quad (2)$$

with V_x, V_y and V_z the time-average velocity components and σ_x, σ_y and σ_z the standard deviation of the velocity components for each point.

While the ADV allows to collect the three velocity components on specific profiles, the Particle Image Velocimetry method (2C-2D PIV) records two components of the velocity on whole planes. This allows the estimation of flow topology, distribution of 2D-average velocity and 2D-turbulent kinetic energy throughout the whole pool. The flow was illuminated by a Nd-YAG laser (Quantel EverGreen, 200 mJ/pulse) in a plane parallel to the channel bed of the fishway located at Z/b = 2, and recorded by a camera of 4920 x 3280 pixels with a Nikon objective of 50 mm. 2,000 instantaneous fields were recorded per case, which is sufficient for statistical estimations. The 2D time-average velocity magnitude (3) and 2D turbulent kinetic energy (4) were calculated as given below:

$$\overline{||V||_{2D}} = \sqrt{\overline{V_x(x,y,z)} + \overline{V_y(x,y,z)}} \quad (3)$$

$$k_{2D} = \frac{1}{2}\left(\sigma_x{}^2(x,y,z) + \sigma_y{}^2(x,y,z)\right) \quad (4)$$

with V_x and V_y the time-average velocity components and σ_x and σ_y the standard deviation of the velocity components for each point.

3 RESULTS

The results for water depth as a function of slope and flowrate are presented in this section. The velocity magnitude (either 2D or 3D) and the turbulent kinetic energy are showed as well.

The water depth was recorded in the middle of the pool (Figure 2).

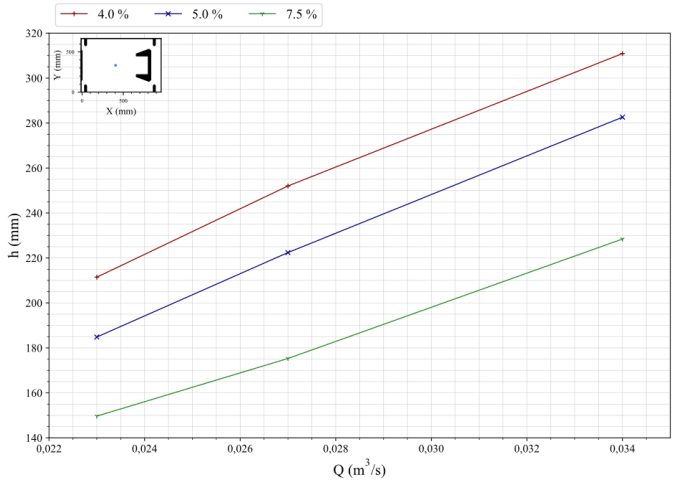

Figure 2. Water depth in the middle of the pool for three slopes (4%, 5% and 7.5%). The inset (top left-hand side corner) shows the location of the sampling point, seen from above.

The evolution of the depth is similar for all slopes: the flow rise involves an increase in water height. Since the slots do not widen between the experiments, the extra flow is converted into depth. For a given flow, the water height is greater for gentler slopes. Less water is retained in each pool when the slope is steep.

The velocity magnitude for two components was recorded for the reference case (s = 4%, Q = 0.034 $m^3 \cdot s^{-1}$) at Z/b = 2 for the whole plane using PIV and on specific profiles using an ADV probe (Figure 3 and Figure 4, respectively).

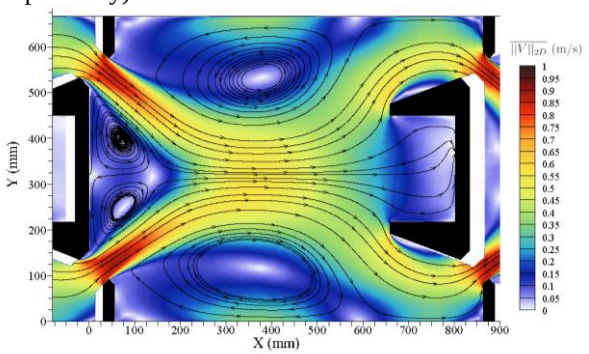

Figure 3. Time-average 2D-velocity magnitude and streamlines for the plane Z/b = 2, for the reference case using PIV

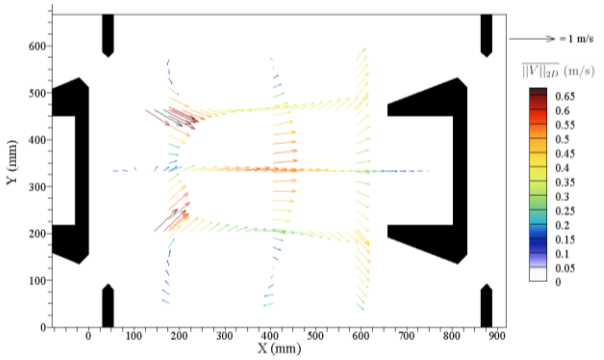

Figure 4. Time-average 2D-velocity magnitude for specific profiles in Z/b = 2, for the reference case using ADV

The velocity magnitude and streamlines from PIV experiments (Figure 3) give an overview of the flow characteristics occurring inside a VDSF. There is no information in the white areas due to the perspective from the camera used in the PIV experiments. The maximum velocity was attained in the slots, with 0.85-0.9 $m \cdot s^{-1}$. The average trajectories inside the pool describe a stretched "X" defined by the slots surrounding the pool. Constrained by the mean trajectories, 5 recirculation areas exist: two are located near the walls of the VDSF, with opposite flowing directions. The recirculation on the right-hand side (looking downstream) is rotating clock-wise while the one on the left-hand side is rotating counterclockwise. Another recirculation area is located in the middle of the following central baffle. The last two are positioned behind the previous central baffle, each one fed by the jet coming from the closest slot.

The results coming from the ADV probe (Figure 4) corroborate the PIV results. The vectors are tallest in the jets after the slots and the side recirculation areas can be seen from the direction of the vectors in all but one profile: the middle longitudinal one, which is the axis of symmetry.

The time-average velocity was also recorded for other flowrates (Q = 0.023 $m^3 \cdot s^{-1}$ and Q = 0.027 $m^3 \cdot s^{-1}$) for the referenced slope (s = 4%). Figure 5 presents the time-averaged velocity magnitude (3 components) for one specific profile (profile C, as can be seen in the top right-hand side corner of Figure 5) using the ADV probe for the three flowrates. The profile C is located at half the water depth of the middle of the pool for each flowrate, which happens to be at Z/b = 2 for the reference case.

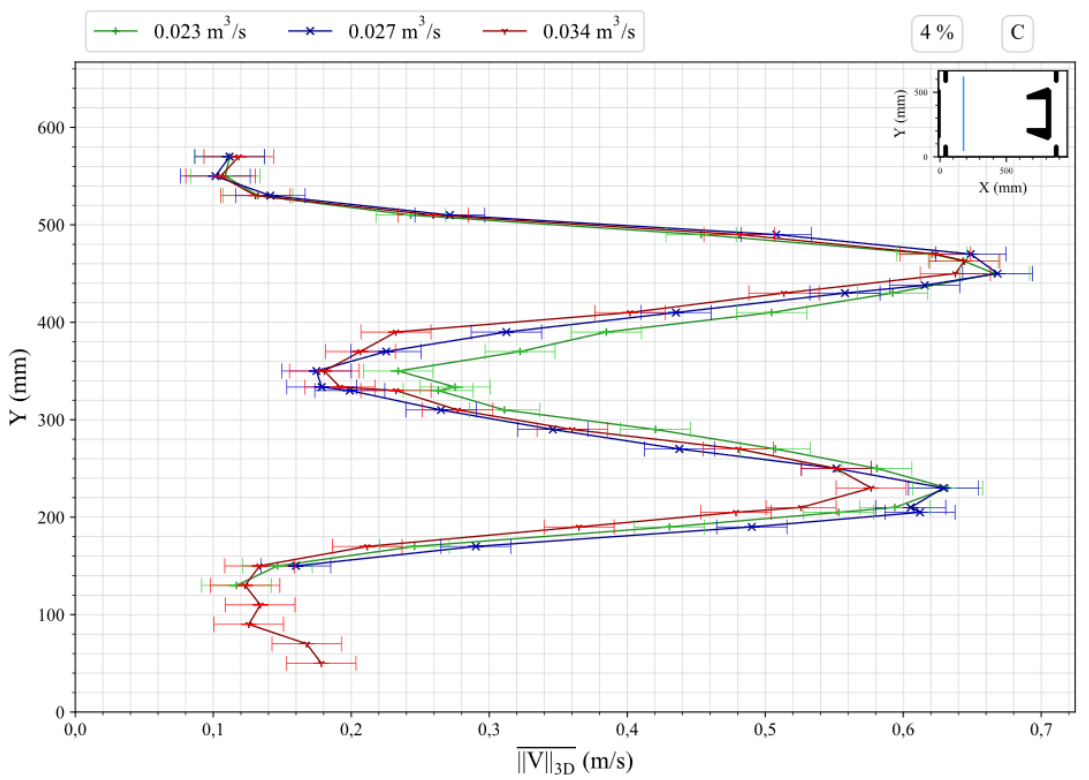

Figure 5. Time-averaged 3D-velocity magnitude for the profile C for a slope of s = 4% and for three flowrates. The inset (top red-hand side corner) shows the location of the sampling profile, seen from above.

The reference flowrate is Q = 0.034 $m^3 \cdot s^{-1}$, the red curve. For all three flowrates, the velocity magnitude presents two peaks, consistent with the two jets coming from the slots. The three velocity magnitude values are similar to one another, indicating that the flowrate does not impact the velocity in this location. At half the water depth, velocities are thus comparable, regardless of the flowrate.

The time-average velocity was recorded as well for several slopes (s = 4% (the reference case), 5% and 7.5%) for the reference flowrate (Q = 0.034 $m^3 \cdot s^{-1}$). Figure 6 presents the time-averaged velocity magnitude (3 components) for profile C using the ADV probe for the three slopes.

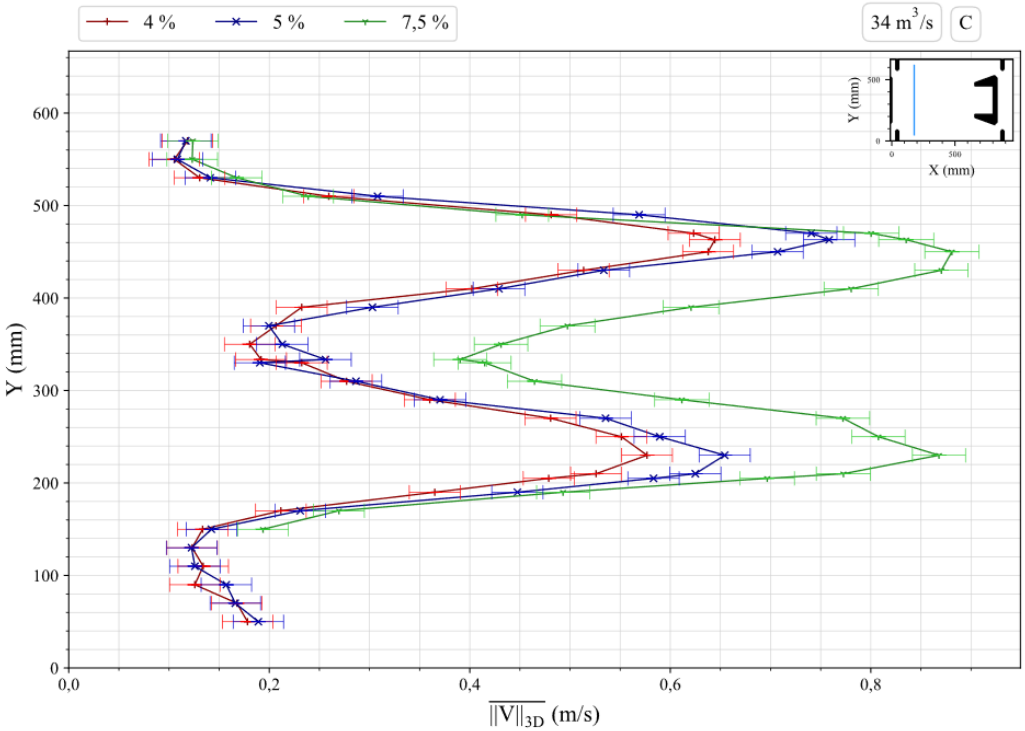

Figure 6. Time-averaged 3D-velocity magnitude for the profile C for a flowrate of Q = 0.034 $m^3 \cdot s^{-1}$ and for three slopes. The inset (top red-hand side corner) shows the location of the sampling profile, seen from above.

The reference slope is s = 4%, the red curve. The profile presents the same two peaks consistent with the jets as in the Figure 5, however value discrepancies can be observed. Velocities at profile C for the 5% slope are comparable to the ones at reference slope (4%). The velocity values at the higher slope (7.5%) are overall higher than those at lower slopes, for almost all Y values: not only are the peak values greater, but the velocity magnitude in the recirculation areas between the two jets is higher as well. Velocity inside a VDSF is thus dependent on the slope.

The turbulent kinetic energy was estimated from the velocity recordings from PIV (2 components) and AVD (3 components) measurements. The 2D-turbulent kinetic energy for the reference case (s = 4% and Q = 0.034 $m^3 \cdot s^{-1}$) derived from PIV results can be seen below on Figure 7.

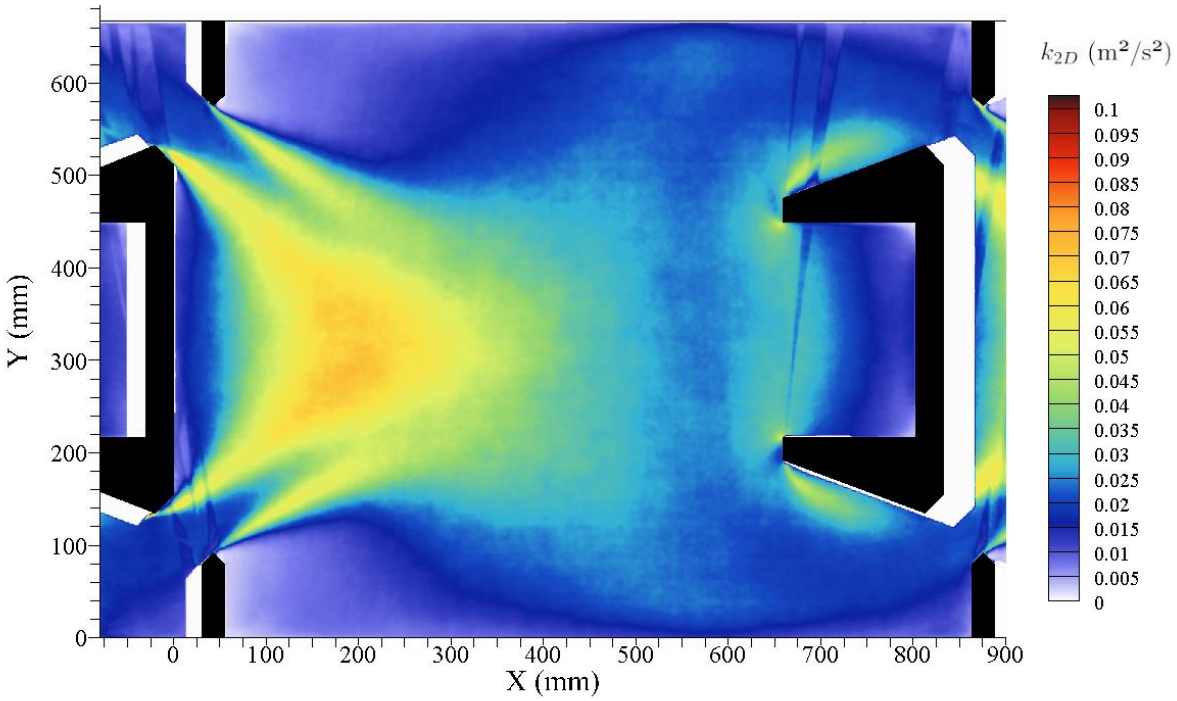

Figure 7. 2D-turbulent kinetic energy in the plane Z/b = 2 from PIV results for the reference case (the "artefacts" seen on the turbulent kinetic energy field come from laser reflections on some part of the prototype)

The PIV experiments allow an overview of the distribution of the 2D-kinetic turbulent energy throughout the pool. The area presenting the highest values is located downstream of the central baffle. Its presence there underlines a phenomenon completely overshadowed by the time-average velocity values and the mean velocity field presented earlier on (Figure 3): the two jets are not constant; they are wavering back and forth. The highest value of turbulent kinetic energy is thus at the meeting area between the two jets. There are also some presences of fluctuation adjacent to the edges of the following central baffle.

The turbulent kinetic energy was studied for the three flowrates (Q = 0.023 $m^3 \cdot s^{-1}$, Q = 0.027 $m^3 \cdot s^{-1}$ and Q = 0.034 $m^3 \cdot s^{-1}$) for the referenced slope (s = 4%). Figure 8 presents the 3D-turbulent kinetic energy for the profile C for the three flowrates.

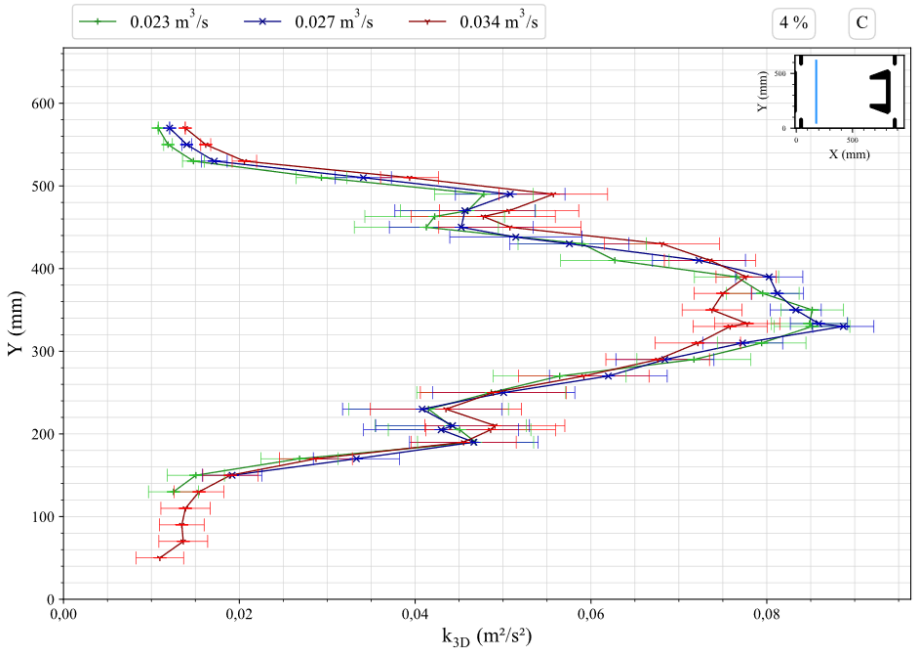

Figure 8. 3D-turbulent kinetic energy for the profile C for a slope of s = 4% and for three flowrates. The inset (top red-hand side corner) shows the location of the sampling profile, seen from above.

The reference flowrate is Q = 0.034 $m^3 \cdot s^{-1}$, the red curve. For all three flowrates, the turbulent kinetic energy presents three peaks; two of small amplitude and a bigger one in the middle. The two smaller peaks are related to the external sides of the jets. The fluctuation in the middle of the jets is reduced compared to the one on the sides, hence the higher value of turbulent kinetic energy on the sides. The peak in the middle is related to the meeting area of the two jets. The three turbulent kinetic energies profiles are similar to one another, with a slightly lower middle peak for the higher flowrate (reference case). Thus, at half the water depth, the turbulent kinetic energy profiles are comparable, regardless of the flowrate.

The turbulent kinetic energy was recorded as well for several slopes (s = 4% (the reference case), 5% and 7.5%) for the reference flowrate (Q = 0.034 $m^3 \cdot s^{-1}$). Figure 9 presents the 3D-turbulent kinetic energy for the profile C using the ADV probe.

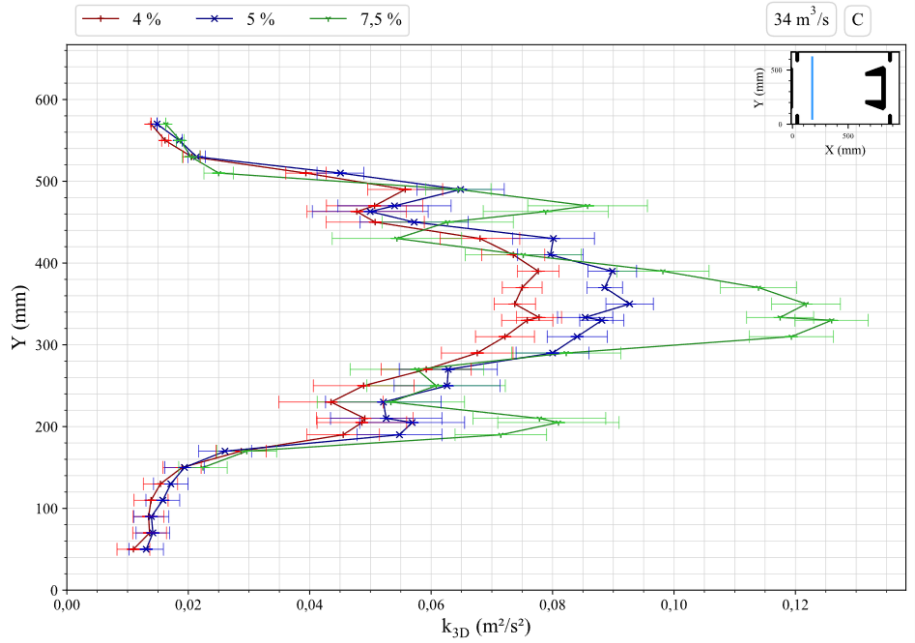

Figure 9. 3D-turbulent kinetic energy for the profile C for a flowrate of Q = 0.034 $m^3 \cdot s^{-1}$ for the three slopes. The inset (top red-hand side corner) shows the location of the sampling profile, seen from above.

The reference slope is s = 4%, the red curve. The profile presents the same three peaks consistent with the jets as in the Figure 8, however value and shape discrepancies can be observed. Turbulent kinetic energy for the 5%-slope presents the same outline as the ones for the reference slope (4%), but with higher values. Turbulent

kinetic energy for the higher slope (7.5%) however, has sharper peaks: the two smaller ones are more defined and the middle one has a high value. Thus, except close to the side walls, the energy is higher for a steeper slope. Furthermore, the steeper the slope, the more defined the peaks are.

4 CONCLUSION

This study focused on the turbulent flow occurring inside a vertical double slot fishway by means of experimental data. Three types of data were computed by use of a laboratory 1:6 replica of an existing VDSF: the water depth in the pools, the velocity components and the turbulent kinetic energy. The distribution of the velocity and the turbulent kinetic energy throughout the pool was presented for the reference case. The maximum velocity is attained in the slots, since the cross-section is reduced. The maximum turbulent kinetic energy is located behind the previous central baffle and is consistent with the wavering of the jets. In addition, the influence of slope and flowrate on those two measures were also studied. It appeared that while the flowrate does not have a decisive impact on those, the slope does. The steeper the slope, the higher the velocity and the turbulent kinetic energy are. Those conclusions will later on be linked to experimental data from the 1:1 reference VDSF in Malause and to fish swimming capabilities data, to determine the impact of scaling on the values and the correspondence with fish behaviour.

5 ACKNOWLEDGMENTS

This work was funded by the French Biodiversity Agency (OFB). The authors acknowledge the financial support of the CPER-FEDER of the Nouvelle-Aquitaine region for the environmental hydrodynamic platform (pHE).

REFERENCES

Ballu, A. (2017). *Étude numérique et expérimentale de l'écoulement turbulent au sein des passes à poissons à fentes verticales. Analyse de l'écoulement tridimensionnel et instationnaire*. PhD thesis. Université de Poitiers.

Ballu, A., Pineau, G., Calluaud, D., & David, L. (2017). Characterization of the flow in a Vertical Slot Fishway with macro-roughnesses using unsteady (URANS and LES) simulations. *37th IAHR World Congress*, *August*.

Ballu, A., Pineau, G., Calluaud, D., & David, L. (2019). Experimental-Based Methodology to Improve the Design of Vertical Slot Fishways. *Journal of Hydraulic Engineering*, *145*(9), 04019031. https://doi.org/10.1061/(asce)hy.1943-7900.0001621

Bombač, M., Novak, G., Mlačnik, J., & Četina, M. (2015). Extensive field measurements of flow in vertical slot fishway as data for validation of numerical simulations. *Ecological Engineering*, *84*(February), 476–484. https://doi.org/10.1016/j.ecoleng.2015.09.030

Bombač, M., Novak, G., Rodič, P., & Četina, M. (2014). Numerical and physical model study of a vertical slot fishway. *Journal of Hydrology and Hydromechanics*, *62*(2), 150–159. https://doi.org/10.2478/johh-2014-0013

Calluaud, D., Cornu, V., Baran, P., & David, L. (2014). Relationship between fish behavior turbulence and unsteady flow in experimental vertical slot fishways. *10th International Symposium on Ecohydraulics, At Trondheim, Norway*, *June*, 1–4.

Clay, C. H. (1995). Design of fishways and other fish facilities - 2nd edition. In *Design of Fishways and Other Fish Facilities*. https://doi.org/10.1201/9781315141046

Fujihara, M., Fukushima, T., & Tachibana, K. (2003). Numerical Investigations of Flow in Vertical Single- and Double-slot Fishways. *Transactions of Irrigation, Drainage and Reclamation Engineering*, *223*, 79–88.

Goring, D. G., & Nikora, V. I. (2002). Despiking Acoustic Doppler Velocimeter Data. *Journal of Hydraulic Engineering*, *128*(1), 117–126. https://doi.org/10.1061/(asce)0733-9429(2002)128:1(117)

Huang, Z. (2020). Preliminary design of laboratory experiment on flow pattern in natural-like fish way ponds. *Journal of Physics: Conference Series*, *1600*(1). https://doi.org/10.1088/1742-6596/1600/1/012060

Klein, J., & Oertel, M. (2016). Vertical Slot Fishway : Evaluation of numerical model quality. *International Junior Researcher and Engineer Workshop on Hydraulic Structures*. https://doi.org/10.15142/T3R599

Stamou, A. I., Mitsopoulos, G., Rutschmann, P., & Bui, M. D. (2018). Verification of a 3D CFD model for vertical slot fish-passes. *Environmental Fluid Mechanics*, *18*(6), 1435–1461. https://doi.org/10.1007/s10652-018-9602-z

Zhao, H., Xu, Y., Lu, Y., Lu, S., Dai, J., & Meng, D. (2022). Numerical Study of Vertical Slot Fishway Flow with Supplementary Cylinders. *Water*, 1–16.